ACS APPLIED MATERIALS & INTERFACES

Research Article

www.acsami.org

High-Performance Lithium Storage Achieved by Chemically Binding Germanium Nanoparticles with N-Doped Carbon

Ying Xiao and Minhua Cao*

Key Laboratory of Cluster Science, Ministry of Education of China, Beijing Key Laboratory of Photoelectronic/Electrophotonic Conversion Materials, Department of Chemistry, Beijing Institute of Technology, Beijing 100081, P. R. China

Supporting Information

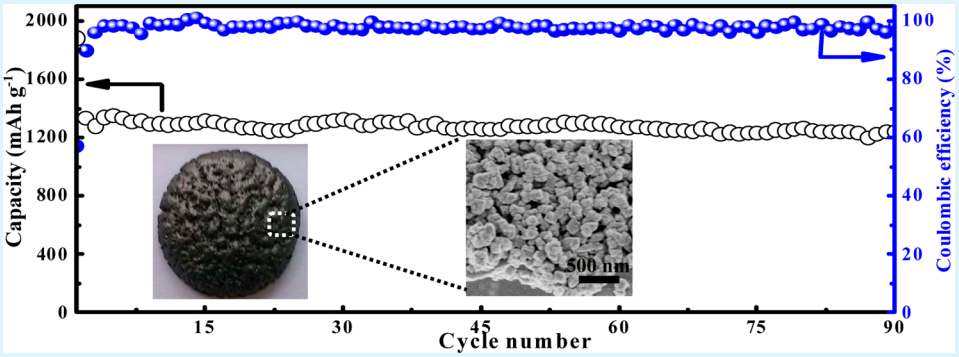

ABSTRACT: Germanium (Ge) is a promising anode material for lithium ion batteries due to its high theoretical capacity. However, its poor cycling stability associated with its large volume changes during discharging and charging processes are urgent problems to solve. This provides opportunities to engineer materials to overcome these issues. Here, we demonstrated a facile and scalable method to synthesize Ge nanoparticles/N-doped carbon monolith with a hierarchically porous structure. The combination of a solvothermal method and annealing treatment results in a well-connected three-dimensional N-doped carbon network structure consisting of Ge nanoparticles firmly coated by the conducting carbon. Such a hierarchical architecture features multiple advantages, including a continuous conductive carbon network, binding the Ge nanoparticles with carbon through a Ge−N chemical bond, and a porous structure for alleviating volume expansion of Ge particles. When serving as an anode for lithium ion batteries, the as-formed hybrid displays high capacities up to 1240.3 mAh g^{-1} at 0.1 A g^{-1} and 813.4 mAh g^{-1} at 0.5 A g^{-1} after 90 cycles, and at the same time, it also exhibits good cycling stability and excellent rate capability.

KEYWORDS: *germanium, monolith, porous structure, anode, lithium ion batteries*

1. INTRODUCTION

Lithium ion batteries (LIBs) have intensively gained attention as energy storage devices for applications such as popular consumer electronics, electric vehicles (EVs), hybrid electric vehicles (HEVs), and so on.[1−3] Germanium (Ge)-based materials have been considered as promising anodes in LIBs to replace the graphite anode because of their appealing advantages, including high theoretical capacity (about 1600 mAh g^{-1}), excellent lithium conductivity, and high electrical conductivity.[4−6] Nevertheless, the satisfactory performance of pure Ge material is still hampered by some issues. Ge usually suffers from severe capacity fading and short cycle life during discharge/charge process, which mainly arise from its sever volume change during the insertion and extraction of lithium. Subsequently, the pulverization of the electrode and the loss of electrical contact occur during the cycling process, leading to the poor lithium storage performance.[7,8] Therefore, numerous efforts have been focused on solving these problems, such as decreasing the crystallite size to the nanoscale, hybrizing with carbon, alloying with metals, and designing porous structure.[9−14]

The carbon materials play a vital role in the material and scientific fields. On the one hand, they can be used as electrodes applied in LIBs by the merits of low cost, high conductivity, and relative safety.[15,16] On the other hand, carbon is considered to be a good matrix to accommodate the volume change for many metals or metal oxides during the discharge/charge process in LIBs owing to its favorable flexibility and conductively.[17−19] However, the low theoretical capacity (372 mAh g^{-1}) and the poor rate capability of traditional carbon have greatly limited its practical application. Thus, many strategies have been developed to solve these problems. Among all the methods, doping N and hybrizing with other materials of higher theoretical capacities are the most popular and effective approaches. More specifically, the N-doping can generate more

Received: May 9, 2014
Accepted: June 27, 2014
Published: June 27, 2014

defects, offering more active sites, and thus enhance the interaction between the carbon and lithium, benefiting the lithium diffusion and transfer.[20,21] The introducing of materials of high theoretical capacity can effectively improve the final lithium storage capacity of the materials. Therefore, combining the N-doped carbon with materials of high theoretical capacity will not only increase the lithium storage capacity but also effectively release the volume expansion of the resultant hybrids efficiently and then improve the cycling stability.[4−6,20−24]

In view of the features of Ge- and N-doped carbon in the field of LIBs, in this work, we designed a feasible method to fabricate Ge nanoparticles (NPs)/N-doped carbon monolith with a hierarchically porous structure (named as Ge@C−N). We introduce a two-step method to realize the ideal structure with Ge NPs uniformly embedded in a well-connected three-dimensional N-doped carbon network. The important step of this method lies in the solvothermal process, which ensures a homogeneous precursor. The subsequent reducing−annealing process for the precursor yields the Ge NPs embedded in nitrogen-doped porous carbon. When serving as an anode for LIBs, the resultant hybrid exhibits perfect lithium storage performance in terms of specific capacity, cycling stability, and rate capability. It can display specific capacities up to 1240.3 mAh g^{-1} at a current density of 0.1 A g^{-1} and 813.4 mAh g^{-1} at a high current density of 0.5 A g^{-1} after 90 discharge−charge cycles. The superior performance may originate mainly from its hierarchical architecture features, including a continuous conductive carbon network, binding the Ge NPs with carbon through Ge−N chemical bond, and a porous structure for alleviating the volume expansion of Ge particles.

2. EXPERIMENTAL SECTION

Synthesis of Porous Ge@C−N Hybrid. A 1 mmol portion of ascorbic acid was added into 10 mL of 0.05 M $GeCl_4$ solution and 40 mL of ethanol. After stirring for 20 min, 2 mL of N_2H_4 was added dropwise into the as-obtained solution. Subsequently, the prepared mixture was treated at 120 °C for 24 h by solvothermal reaction. After cooling to room temperature, the yellow bulk precursor can be obtained, which was annealed at 600 °C for 2 h under Ar/H_2 atmosphere ($Ar:H_2$ = 93%:7%, by volume) with a heating rate of 5 °C min^{-1} to generate the final typical porous Ge@C−N hybrid. For comparison, the Ge@C−N hybrids with different carbon contents were obtained by annealing the same precursor at 500 and 700 °C for 2 h under Ar/H_2 atmosphere. The Ge/C sample was formed by annealing the precursor at 750 °C for 2 h under Ar/H_2 atmosphere, which was synthesized without the addition of N_2H_4 while the other conditions were kept similar to those of the typical sample (a temperature lower than 750 °C cannot obtain the target product). The bare Ge was fabricated by reducing the commercial GeO_2 at 750 °C for 2 h under Ar/H_2 atmosphere.

Characterizations. The composition of the samples was obtained by powder X-ray diffraction (XRD) using a Bruker D8 X-ray power diffactometer with a voltage and current of 40 kV and 40 mA, respectively. Transmission electron microscopy (TEM) (H-8100, 200 kV accelerating voltage) and the field emission scanning electron microscopy (FE-SEM) (Hitachi S-4800 SEM unit) were used to investigate the morphology of the samples. The surface composition of the sample was analyzed by X-ray photoelectron spectra (XPS) (ESCALAB 250 spectrometer (PerkinElmer)). Raman spectra were recorded by an Invia Raman spectrometer, using an excitation laser of 633 nm. The carbon and nitrogen contents were determined using the combustion method by an elemental analyzer (Vario EI). The Brunauer−Emmett−Teller (BET) surface area of as-formed samples was measured using a Belsorp-max surface area detecting instrument by N_2 physisorption at 77 K.

Electrochemical Measurements. Electrochemical performance was evaluated by using coin cells (CR2025) on a multichannel battery testing system (LAND CT2001A). The active material, acetylene black, and CMC binder were mixed in a weight ratio of 70:15:15 for the fabricating of working electrode. The mixture was ground and a slurry made in a mortar using deionized water as solvent. Subsequently, the slurry was uniformly pasted on the Cu foil; the typical electrode was dried at 120 °C for 36 h under vacuum before being assembled into a coin cell in an argon-filled glovebox. Lithium foil was used as the counter electrode. The electrolyte was used with 1 M $LiPF_6$ in ethylene carbonate (EC)/dimethyl carbonate (DMC)/diethyl carbonate (DEC) (1:1:1 by volume). The loading of the active electrode was 0.91 mg cm^{-2}. Cyclic voltammetry (CV) curves were recorded using a CHI-760E workstation at a scanning rate of 0.1 mV s^{-1}. The impendence spectra were obtained by applying a sine wave with amplitude of 5 mV over the frequency range from 100 kHz to 0.01 Hz.

3. RESULTS AND DISCUSSION

A schematic illustration for the fabrication process of the porous Ge@C−N hybrid is shown in Figure 1, which involves

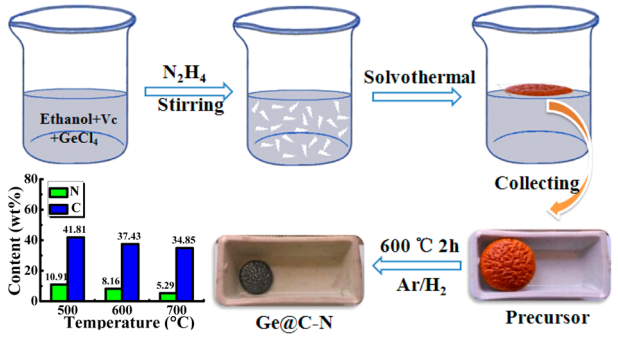

Figure 1. Schematic representation of the fabrication process of the porous Ge@C−N hybrid and carbon and nitrogen contents in the hybrids obtained at different temperatures.

dehydration, polymerization, and carbonization of the ascorbic acid under solvothermal conditions and heat treatment. Briefly, a white suspension was first obtained by the hydrolysis of $GeCl_4$ in ethanol solution of ascorbic acid with some content of N_2H_4 (80%). Here, it should be noted that the ascorbic acid was selected as carbon resource; N_2H_4 with 80% content was chosen as nitrogen resource and at the same time it can also promote the hydrolysis of $GeCl_4$. Then, the as-obtained white suspension was transferred into an 80 mL Teflon-lined stainless-steel autoclave and treated at 120 °C with solvothermal reaction. After that an orange, disk-shaped monolith was observed floating on the surface of the clear liquid instead of a powder precipitate at the bottom of the Teflon cup in the usual cases, which will act as a precursor for the final product. Lastly, this orange monolith was placed in a porcelain boat and subjected to calcining in a furnace under a reducing atmosphere. The reduction−carbonization process leads to the formation of a porous Ge@C−N hybrid. During this process, the monolith precursor underwent remarkable size shrinkage owing to the release of some small molecular byproducts, and its color has also changed to dark gray. Additionally, it should be noted that by adjusting the annealing temperature, different carbon contents of hybrids could be controllably obtained. The mass percentages of carbon and nitrogen of all the samples revealed by CHN element analysis are displayed in the left part of Figure 1. It can be clearly seen

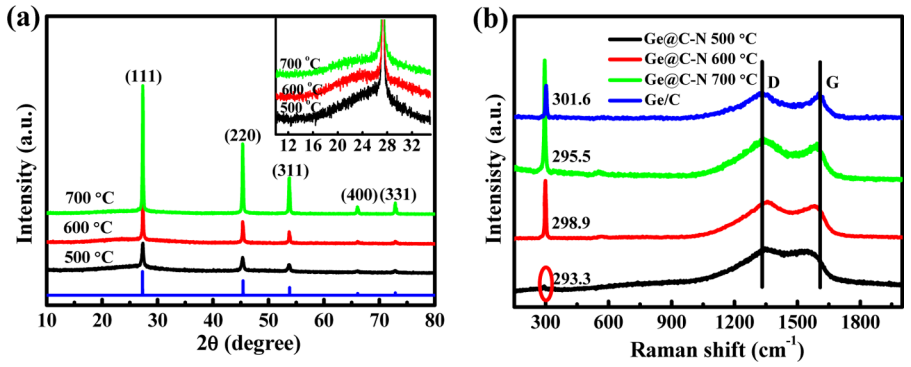

Figure 2. (a) XRD patterns of the resultant Ge@C−N hybrids formed under different temperatures. (Inset) XRD patterns in the angle range of 10°−35°. (b) The Raman spectra of the resultant Ge@C−N hybrids formed under different temperatures along with the Ge/C hybrid.

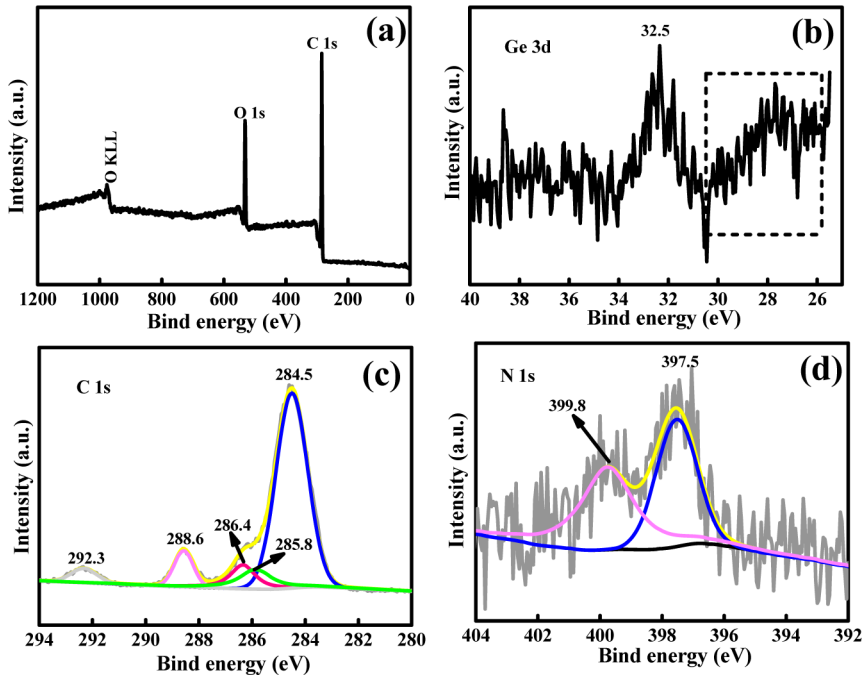

Figure 3. XPS spectra of the typical Ge@C−N hybrid: (a) the survey spectrum and (b−d) the high-resolution spectra of Ge 3d, C 1s, and N 1s, respectively.

that compared to C, the N content decreases more evidently with the increase of the annealing temperature. The possible reason may be related to the following several aspects. First, some of the sp^3-hybridized C−N bonds may be replaced by relatively stable sp^2-hybridized C−C bonds at higher temperature due to the higher bonding energy of C−C. On the other hand, at high temperatures, some instable nitrogen species could form stable N_2 molecules, which immediately get away from the reaction system without incorporating into the carbon structure,[25−27] and at the same time the high temperatures generally favor the formation of high crystallinity carbon, which leads to difficult incorporation of foreign elements into its structure. Additionally, the carbonization of the organic species in the precursor and the carbothermal reduction of the Ge−O by the as-formed carbon became more complete upon the increasing of the annealing temperature, resulting in the mass loss of the carbon to some extent. During these processes, the loss level of N effected by the temperature was higher than that of C, thus leading to the increased C/N ratio with the temperature increase.

The crystallographic structure and the composition of the products were first examined by an X-ray diffraction (XRD) technique. As shown in Figure S1 (Supporting Information), the XRD pattern of the precursor shows only two broad reflections at around 11.7° and 24.7°, and no other diffraction peaks corresponding to the crystalline phase are observed, indicating the amorphous structure of the precursor. After heat treatment at different temperatures in H_2/Ar gas, the amorphous precursor has transformed into crystalline products, as confirmed by Figure 2a. For each case, all distinct and intense diffraction peaks match well with a cubic phase Ge (JCPDS No. 65-0333). The main peaks located at $2\theta \approx 27.3°$, 45.3°, 53.7°, 66.0°, and 72.9° can be assigned to (111), (220), (311), (400), and (331) reflections of cubic Ge, respectively. Meanwhile, a weak and broad peak between 18° and 32° could be clearly observed for all the samples (the inset in Figure 2a), which can be ascribed to the carbon in the hybrids. The sharp diffraction peaks not only imply the good crystallization of the samples, but also confirm the increased crystallization with the temperature increasing. In addition, the calculated grain sizes of

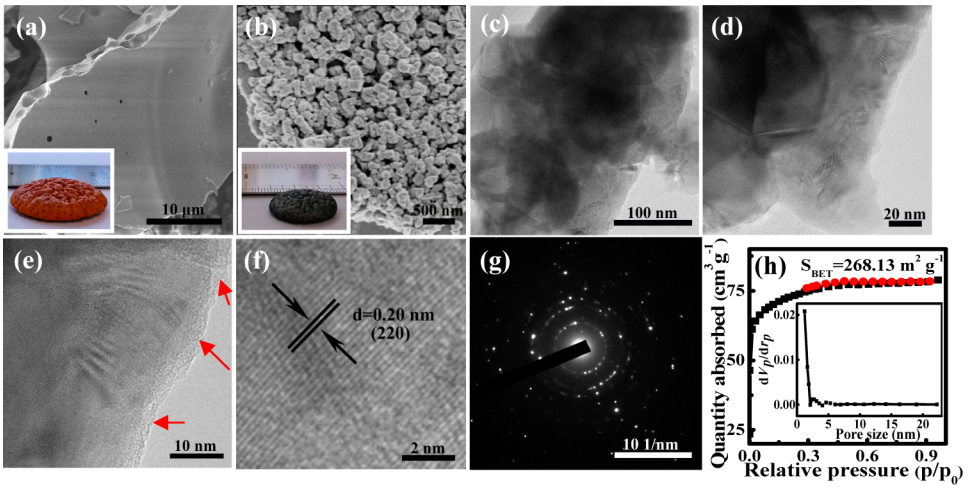

Figure 4. FE-SEM images of (a) the precursor and (b) the typical Ge@C−N hybrid. The inset ones corresponded to the sample's optical photos. (c−e) The TEM images of the typical Ge@C−N hybrid. (f) The HRTEM image and (g) the corresponded SAED pattern of the typical Ge@C−N hybrid. (h) Nitrogen adsorption−desorption isotherms and the corresponded pore-size distribution of the as-resultant typical Ge@C−N hybrid.

Ge according to the Scherrer equation based on the (220) peak were 28.9 nm for 500 °C, 63.2 nm for 600 °C, and 81.4 nm for 700 °C, and the electrochemical performance of these three samples will be studied in the following section. Besides, Raman spectra of all the samples show similar peaks in the range of 150−2000 cm^{-1}. As displayed in Figure 2b, for all the samples, the peak in the range of 290−305 cm^{-1} can be assigned to the optical mode of crystalline germanium. This peak for all the Ge@C−N hybrids shows a slight shift compared to that of the Ge/C hybrid, which may result from the interaction between Ge- and N-doped carbon.[28] Additionally, those two peaks centered at about 1583 and 1352 cm^{-1} correspond to the G- and D-bands of carbon, respectively, which are the characteristic peaks for carbon materials.[15−17] Generally, the G-band corresponds to the Raman-allowed optical mode E_{2g}, which is related to the vibration in all sp^2-band carbon atoms in a two-dimensional hexagonal lattice, while the D-band is associated with sp^3-hybridized carbon, structural defects, or amorphous carbon.[29,30] According to the literature,[31,32] the intensity ratio of D-band to G-band (I_D/I_G) in the Raman spectrum could be used to determine the defect and disorder of the graphitized structure and the fraction of sp^3/sp^2-bonded carbon. In our case, the intensity ratios (I_D/I_G) in the Ge@C−N hybrids are 1.46 for 500 °C, 1.05 for 600 °C, and 1.02 for 700 °C, all of which are larger than that in the Ge/C hybrid (0.99), suggesting the existence of defects after N-doping and the increasing of graphitization degree with the increase of the annealing temperature. From the CHN elemental analysis results (Figure 1), we know that different calcining temperatures could lead to different N contents. Generally, the introduction of heteroatoms would lead to the formation of defects in the host materials. Therefore, the N-doping in our work may result in the formation of more defects, which is considered to provide more reversible sites for Li storage, contributing to the overall capacity when the product is used as electrode in LIBs. Furthermore, the G- and D-bands in different Ge@C−N samples both exhibit an obvious shift compared to those of the Ge@C, which may be ascribed to the C−C expansion or contraction and the changes in electronic structure resulting from different N contents according to the previous reports.[33−35] All of these results indicate the formation of carbon and successful N-doping, which undoubtedly enhance the conductivity of the Ge and induce more defects, enduing the resultant hybrid with excellent electrochemical performance.

To further determine the composition and chemical state of the sample, X-ray photoelectron spectroscopy (XPS) measurement was conducted on the sample obtained at 600 °C (we name this sample as the typical Ge@C−N hybrid in the following discussion). As shown in the survey XPS spectrum (Figure 3a), those three obvious signals can be assigned to C and O elements, while the N and Ge peaks are not distinct, which may due to these two elements being firmly embedded in the carbon matrix. However, their high-resolution spectra confirm the existence of Ge and N in this hybrid. The XPS spectrum (Figure 3b) for Ge 3d shows a broad peak with binding energy less than 30 eV, which can be assigned to the Ge phase. The peak at 32.5 eV can be attributed to the Ge−O bond, which may result from the local heating effect during the test process.[36] Figure 3c shows the fitted high-resolution spectra of the C 1s core-level, which display five peaks. The peak at around 284.5 eV (69.1 atom %) can be assigned to C−C in the carbon. Other peaks at 285.8 eV (9.9 atom %), 286.4 eV (9.2 atom %), 288.6 eV (7.7 atom %), and 292.3 eV (4.1 atom %) can be attributed to C−N, C−O, C═O, and $\pi-\pi^*$, respectively.[37] As for the N 1s spectra (Figure 3d), the peaks located at 399.8 (53.4 at%) and 397.5 eV (46.6 at%) correspond to the pyrrolic nitrogen and Ge−N bond, respectively.[38,39] Therefore, Raman and XPS both confirmed the presence of metal−N and C−N bonds, which are believed to be indispensable for the high electrochemical performance.

The microstructure of the resultant samples was examined by field-emission scanning microscopy (FE-SEM) and transmission electron microscopy (TEM). From the FE-SEM images, it can be seen that the precursor is composed of agglomerates with tens of micrometers (Figure 4a) and the inset clearly displays the optical photo of the precursor monolith with diameter of about 1 in., which exhibits well-defined discal morphology with an orange color. After heat treatment, the agglomerates are relatively uniform in size. In addition, the diameter of the NPs increased with the increasing of the annealing temperature, which will have important effect on the electrochemical performance. The inset image in Figure 4b reveals that the annealed product still exhibits discal

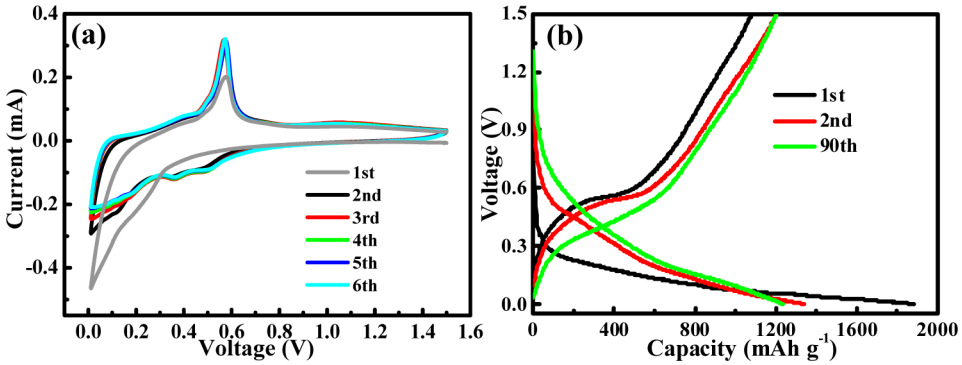

Figure 5. (a) CV curves of the typical Ge@C−N electrode for the first six cycles. (b) Discharge/charge voltage profiles of the typical Ge@C−N electrode at 0.1 A g^{-1} for different cycles.

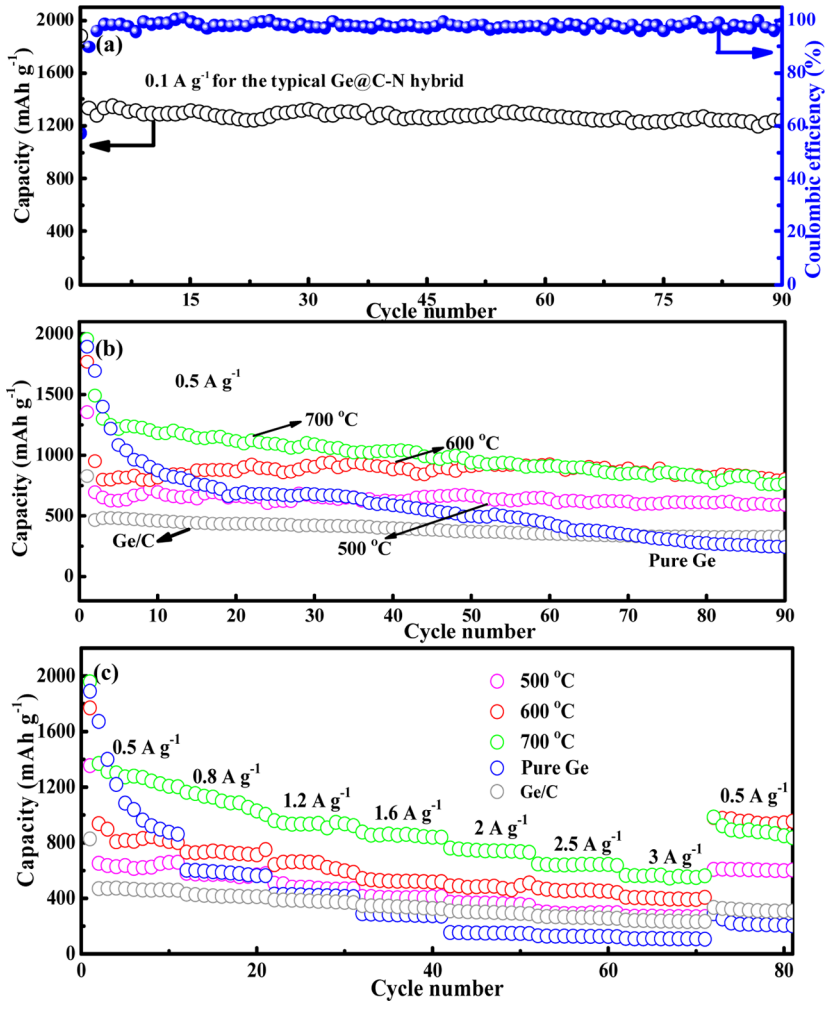

Figure 6. (a) Cycling performance and the corresponding Coulombic efficiency of the typical Ge@C−N electrode at 0.1 A g^{-1}. The cycling performance comparison of Ge@C−N hybrids along with the bare Ge at 0.5 A g^{-1} (b) and at various current densities (c).

monolith morphology with diameter smaller than 1 in., which has a dramatic shrinkage compared to the precursor. Figure 4c−e shows TEM images of the typical Ge@C−N hybrid with different magnifications. More specifically, the Ge NPs have an average diameter of ∼60 nm. Since the carbon was formed synchronously with the Ge NPs, the Ge NPs are in intimate contact with the conductive carbon matrix at both the microscopic and molecular level, which is confirmed by the higher-magnification TEM image (Figure 4e). It can be observed that the Ge NPs were firmly embedded inside a uniform carbon matrix. This unique microstructure would be beneficial for improving the electrochemical performance of the hybrid. Figure 4f shows the high-resolution TEM (HRTEM) image of a single Ge particle, and the lattice fringe with an interplanar distance of 0.20 nm can be attributed to the (220) plane of Ge. The diffraction rings in the selected area electron diffraction (SAED, Figure 4g) indicate the polycrystalline nature of the hybrid. To further examine the porous properties

of the typical Ge@C−N hybrid, N_2 adsorption/desorption isotherm measurements were performed, as shown in Figure 4h. A rapid growing of the adsorption capacity at relatively low pressures ($p/p_0 < 0.1$) and a hysteresis loop at p/p_0 in the range of 0.3−0.9 in the isotherms indicate the presence of mesopores and micropores in this hybrid.[40,41] The corresponding pore size distribution curve also confirms this kind of hierarchically porous structure (see the inset in Figure 4h). Such a porous structure gives rise to a Brunauer−Emmett−Teller (BET) surface area as high as 268.13 $m^2 g^{-1}$. The high surface area may provide a large number of active sites for the electrochemical performance. Furthermore, the pore structure could effectively reduce the diffusion path of lithium ions and electrons in electrode material and increase the electrochemical reaction area, both of which are beneficial for the electrochemical performance.[42,43]

In view of the novel structure and the porous feature of the typical Ge@C−N hybrid, we investigate its electrochemical performance as an anode in LIBs. Figure 5a displayed the cyclic voltammetry (CV) curves of the typical Ge@C−N hybrid obtained with the annealing temperature of 600 °C at a scan rate of 0.1 mV s^{-1} in the range of 0.01−1.50 V, which agree with the previous reports.[10,22,44] A small reduction peak at around 0.3 V in the first cycle could be associated with the formation of a solid electrolyte interphase (SEI) layer. The lithiation peaks at around 0.51, 0.36, and 0.13 V along with the delithiation peaks at about 0.57 V in the different cycles correspond to the phase transition between Ge and Li_xGe alloy.[18,44−46] Additionally, it is worth noting that the CV curves are well-overlapped, implying the good cycling stability of the Ge@C−N electrode during the discharge/charge process. Figure 5b shows the discharge−charge voltage profiles cycled at a current density of 0.1 A g^{-1} with a cutoff voltage window of 0.01−1.50 V vs Li^+/Li. The first lithiation delivers a capacity of 1884.3 mAh g^{-1} and 57.3% of the inserted Li can be reversibly delithiated, giving a charge capacity of 1080.4 mAh g^{-1}. The high capacity loss in the first cycle is also common in other anode materials, which is mainly caused by the formation of the SEI layer solid.[17,47]

Figure 6a shows the cycling performance of the typical Ge@C−N electrode at 0.1 A g^{-1} for a potential window of 0.01−1.50 V. The capacity value was calculated on the basis of the total mass of N-doped C and Ge. It can be seen that the electrode exhibits exceptional cycling stability during 90 charge/discharge cycles with slight capacity decay. It can retain a highly reversible capacity up to 1240.3 mAh g^{-1} after 90 cycles, with a Coulombic efficiency of 98.6%. Figure 6b presents the cycling performance of the Ge@C−N hybrids obtained with different annealing temperatures as well as the bare Ge and Ge/C at 0.5 A g^{-1} (the characterization of Ge/C is shown in Figure S3, Supporting Information). It can be obviously seen that the typical electrode displays relatively excellent capacity retention and cycling performance. It can deliver a lithium storage capacity as high as 813.4 mAh g^{-1} even at 0.5 A g^{-1} after 90 cycles, which exhibits high capacity retention ratios of about 85.6% and 99.8% compared with the 2nd cycle and the 10th cycle, respectively. This capacity is significantly higher than that of the bare Ge (235.5 mAh g^{-1}) and Ge/C hybrid (328.6 mAh g^{-1}) and also higher than those of the hybrids obtained at 500 and 700 °C (597.1 and 738.8 mAh g^{-1}, respectively). In addition, it can also be observed from Figure 6b that the sample annealed at 700 °C exhibits relatively high initial discharge capacity, but its capacity retention ratios are relatively low. The reason may be related to its relatively low carbon and nitrogen contents and larger particle size. From the previous CHN element analysis results, we know that the contents of C and N in the hybrids both decrease, but the N content drops more evidently with the increase of the annealing temperature. The lower C content inevitably increases the Ge content (with high theoretical capacity) in the resultant hybrid, which may result in the higher capacity in the initial cycle; meanwhile, the high temperature results in the larger size of Ge particles accordingly, which is not beneficial for alleviating the volume changes during charge/discharge process, thus leading to poor cycling performance. Moreover, low N-doping content yields fewer defects in the carbon layer, which cannot provide more active sites for the additional Li ion storage. In view of the above aspects, we think that, for the optimal sample annealed at 600 °C, the C/N ratio combined with the Ge particle size may achieve the best balance, which contributes to the final excellent cycling stability and relatively high capacity. Furthermore, it is well-known that the rate capability is an important parameter for practical applications of LIBs, for example, especially for electric vehicles and power tools. Therefore, we evaluated the rate capability of the samples under a wide range of current densities (from 0.5 to 3 A g^{-1}). As displayed in Figure 6c, a capacity of 406.6 mAh g^{-1} for the typical Ge@C−N hybrid electrode can be obtained even at a high current density of 3 A g^{-1}. When the rate comes back to 0.5 A g^{-1}, the capacity of the typical Ge@C−N hybrid can recover to the value similar to the initial one, indicating its excellent capacity capability. Additionally, compared with the bare Ge, Ge/C, the hybrids annealed at 500 and 700 °C, the typical sample exhibits relatively good cycling stability and rate capability under the same test conditions.

To obtain more insight into the superior electrochemical performance of the porous Ge@C−N hybrid, electrochemical impedance spectroscopy (EIS) measurements were conducted. Figure 7a,b displays the Nyquist plots for the typical Ge@C−N hybrid, bare Ge, and Ge/C electrodes after 90 cycles at 0.5 A

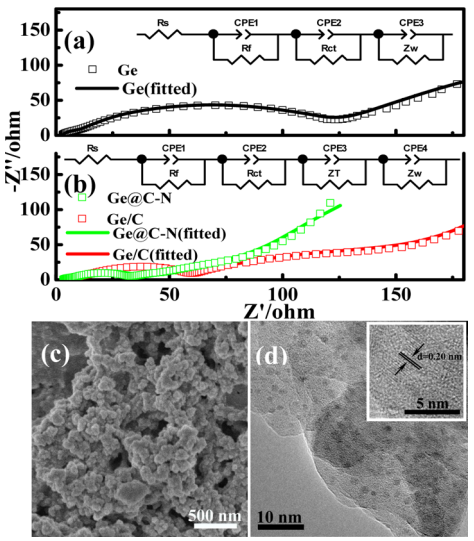

Figure 7. (a, b) Electrochemical impedance spectroscopies of the typical Ge@C−N, bare Ge, and Ge/C electrodes after 90 cycles at 0.5 A g^{-1} along with the corresponding simulation plots. The inset ones are the equivalent electrical circuits for fitting. (c) SEM image and (d) TEM images of the typical Ge@C−N electrode after 90 cycles at 0.5 A g^{-1}. The inset in part d is the corresponding HRTEM image.

g^{-1}. The measured EIS spectra are analyzed and fitted, and an equivalent circuit for this cell is also provided. Generally, the Nyquist plots consist of a depressed semicircle in the high-middle frequency regions followed by a sloping straight line in the low-frequency region. The high-frequency semicircle corresponds to the electrolyte resistance (R_s), while the semicircle at high-middle frequencies can be assigned to the SEI resistance and contact resistance (R_f) and the charge-transfer impedance on electrode−electrolyte interface (R_{ct}). The sloped line in the low frequency region can be ascribed to the typical Warburg impedance (Z_w), which is related to the semi-infinite diffusion of the Li ions in the electrodes. However, for the Ge@C−N and Ge/C samples (Figure 7b), they display an obvious difference in the front part of the Warburg diffusion when compared to the pure Ge (Figure 7a), which can be assigned to the barrier layer diffusion of the Li ions in the current electrodes due to the formation of the barrier layers, and the corresponding impedance is depicted as Z_T.[48] It can be obviously observed that the diameter of the semicircle for the Ge@C−N electrode is much smaller than that of the bare Ge and Ge/C after 90 cycles, indicating the lower charge transfer resistance and an enhanced electric conductivity of the Ge@C−N hybrid.[20,49] This conclusion is also confirmed by the fitted results based on the equivalent circuit depicted in Figure 7a,b (insets). The R_{ct} for the Ge@C−N electrode is 23.3 Ω, which is much smaller than those of the bare Ge (112.2 Ω) and Ge/C (45.7 Ω). These results indicate that N-doped C endows the Ge with a higher conductivity, which can enhance the electrotransport during the electrochemical process.[50] In addition, to provide further insight into the excellent performance of the Ge@C−N hybrid, a SEM study was used to test the morphology of the hybrid electrode after 90 cycles at 0.5 A g^{-1} (Figure 7c). The Ge@C−N electrode almost maintains its overall morphology. The TEM image along with the HRTEM image (Figure 7d) indicated that the Ge NPs changed into ultrafine Ge NPs with a particle size less than 3 nm, which are homogeneously confined in the carbon matrix. Similar to the literature,[51] the homogeneous distribution of Ge NPs may make them connect electrochemically with the carbon more closely, benefiting the charge transfer; meanwhile, the smaller size of the Ge NPs will partially alleviate the volume change and significantly reduce the Li^+ transport path,[52,53] all of which contributed to the final excellent electrochemical performance.

The lithium storage performance for the as-prepared hybrid is superior over most of the previous reports, as listed in Table 1. According to these investigations, we believe that the excellent lithium storage performance of the typical Ge@C−N hybrid may be attributed to the small size of Ge particles, the three-dimensional N-doped carbon network, the chemical bond between Ge and N, and the porous structure. In detail, the small size of the Ge grains could alleviate the volume expansion/contraction during the discharge/charge process to some extent.[59] The coating of carbon could also effectively accommodate the volume change of Ge and limits the agglomeration of Ge NPs.[2] The introduction of N-doped carbon can provide a continuous pathway for electron transport and further buffers the volume change of Ge NPs, improving the elasticity and conductivity of the resultant electrode. Meanwhile, more Li insertion active sites would be produced, owing to more defects originating from the N-doping, which can enhance the lithium storage of the active materials.[17,20] Additionally, the Ge−N chemical bond avoids the aggregation of Ge or Li_xGe_y particles during cycling, which is believed to be beneficial for the excellent electrochemical performance.[2] Finally, the porous structure can increase the contact area of the electrolyte and electrode, reduce the lithium ion diffusion path, and alleviate the strain induced by the volume change during the cycling process.[22,32,49] All of these aspects contribute to the high capacity, cycling stability, and rate capability of the Ge@C−N hybrid.

Table 1. Capacity Comparison of Present Work with Reported Ge-Based Materials

samples	current density (mA g^{-1})	cycle number	capacity (mAh g^{-1})	ref
C/Ge composites	ca. 506	30	545.1	6
porous C/Ge nanowire	160	50	789	7
Ge@CNF@C	50	50	553	18
Ge/SCNT	25	40	417	23
Ge-CNFs	243	100	740	24
Ge@C composite	800	100	734	45
3D Ge/GR composites	160	50	832	50
Ge@GR composites	400	600	675	54
Ge/CNT/Cu foam	150	100	800	55
binder-free Ge-3D GR	437	100	1140	56
Ge@C composite	100	50	579	57
Ge wires/Ge fibers	ca.122	50	1200	58
Ge@C−N	100 (500)[a]	90	1235.0 (813.4)[a]	this work

[a]The cycles in parentheses in row 2 correspond to the capacity values in parentheses in row 4.

4. CONCLUSION

In conclusion, we have developed a facile and scalable approach to prepare Ge@C−N hybrid with a hierarchically porous structure via a solvothermal treatment followed by an annealing process. The resultant Ge@C−N hybrid features multiple advantages, including a continuous electrically conductive carbon network, binding the Ge nanoparticles with carbon through a Ge−N chemical bond, and a porous structure for volume expansion of Ge particles. Compared with the bare Ge, the typical Ge@C−N hybrid exhibits high capacity, good cycling stability, and excellent rate capability under the same test conditions. The unique composition and structure not only can effectively alleviate the stress and accommodate large volume changes upon prolonged cycling but also can provide fast electronic and ionic transfer channels. Besides, the porous structure can reduce the ion transport length and increase the contact area of electrode and electrolyte, yielding more Li^+ crossing the interface. Moreover, the current fabrication method is very simple and highly scalable, which can be extended to other battery electrode material systems.

■ ASSOCIATED CONTENT

Supporting Information

The XRD pattern of the precursor, SEM images for the samples annealed at 500 and 700 °C, and the XRD pattern and SEM image of the Ge/C sample obtained without the addition of N_2H_4. This material is available free of charge via the Internet at http://pubs.acs.org/

AUTHOR INFORMATION

Corresponding Author

*Fax: +86-10-68918572. Tel: +86-10-68918468. E-mail: caomh@bit.edu.cn.

Notes

The authors declare no competing financial interest.

ACKNOWLEDGMENTS

This work was supported by the National Natural Science Foundation of China (21271023, 91022006, and 20973023) and the 111 Project (B07012)

REFERENCES

(1) Yu, L.; Zhang, L.; Wu, H. B.; Zhang, G. Q.; Lou, X. W. Controlled Synthesis of Hierarchical $Co_xMn_{3-x}O_4$ Array Micro-/Nanostructures with Tunable Morphology and Composition as Integrated Electrodes for Lithium-Ion Batteries. *Energy Environ. Sci.* **2013**, *6*, 2664−2671.

(2) Zhou, X. S.; Wan, L. J.; Guo, Y. G. Binding SnO_2 Nanocrystals in Nitrogen-Doped Graphene Sheets as Anode Materials for Lithium-Ion Batteries. *Adv. Mater.* **2013**, *25*, 2152−2157.

(3) Qu, J.; Yin, Y. X.; Wang, Y. Q.; Yan, Y.; Guo, Y. G.; Song, W. G. Layer Structured α-Fe_2O_3 Nanodisk/Reduced Graphene Oxide Composites as High-Performance Anode Materials for Lithium-Ion Batteries. *ACS Appl. Mater. Interfaces* **2013**, *5*, 3932−3936.

(4) Xue, D. J.; Xin, S.; Yan, Y.; Jiang, K. C.; Yin, Y. X.; Guo, Y. G.; Wan, L. J. Improving the Electrode Performance of Ge through Ge@C Core−Shell Nanoparticles and Graphene Networks. *J. Am. Chem. Soc.* **2012**, *134*, 2512−2515.

(5) Seng, K. H.; Park, M. H.; Guo, Z. P.; Liu, H. K.; Cho, J. Self-Assembled Germanium/Carbon Nanostructures as High-Power Anode Material for the Lithium-Ion Battery. *Angew. Chem., Int. Ed.* **2012**, *51*, 5657−5661.

(6) Xiao, Y.; Cao, M. H.; Ren, L.; Hu, C. W. Hierarchically Porous Germanium-Modified Carbon Materials with Enhanced Lithium Storage Performance. *Nanoscale* **2012**, *4*, 7469−7474.

(7) Tan, L. P.; Lu, Z. Y.; Tan, H. T.; Zhu, J. X.; Rui, X. H.; Yan, Q. Y.; Hng, H. H. Germanium Nanowires-Based Carbon Composite as Anodes for Lithium-Ion Batteries. *J. Power Sources* **2012**, *206*, 253−258.

(8) Yang, L. C.; Gao, Q. S.; Li, L.; Tang, Y.; Wu, Y. P. Mesoporous Germanium as Anode Material of High Capacity and Good Cycling Prepared by a Mechanochemical Reaction. *Electrochem. Commun.* **2010**, *12*, 418−421.

(9) Yuan, F. W.; Tuan, H. Y. Scalable Solution-Grown High-Germanium-Nanoparticle-Loading Graphene Nanocomposites as High-Performance Lithium-Ion Battery Electrodes: An Example of a Graphene-Based Platform toward Practical Full-Cell Applications. *Chem. Mater.* **2014**, *26*, 2172−2179.

(10) Li, W.; Zheng, J.; Chen, T. K.; Wang, T.; Wang, X. J.; Li, X. G. One Step Preparation of a High Performance Ge−C Nanocomposite Anode for Lithium Ion Batteries by Tandem Plasma Reactions. *Chem. Commun.* **2014**, *50*, 2052−2054.

(11) Jin, S. X.; Li, N.; Cui, H.; Wang, C. X. Growth of the Vertically Aligned Graphene@Amorphous GeO_x Sandwich Nanoflakes and Excellent Li Storage Properties. *Nano Energy* **2013**, *2*, 1128−1136.

(12) Song, T.; Cheng, H. Y.; Choi, H.; Lee, J. H.; Han, H.; Lee, D. H.; Yoo, D. S.; Kwon, M. S.; Choi, J. M.; Doo, S. G.; Chang, H.; Xiao, J. L.; Huang, Y. G.; Park, W.; Chung, Y. C.; Kim, H. S.; Rogers, J. A.; Paik, U. Si/Ge Double-Layered Nanotube Array as a Lithium Ion Battery Anode. *ACS Nano* **2012**, *6*, 303−309.

(13) Zou, F.; Hu, X. L.; Sun, Y. M.; Luo, W.; Xia, F. F.; Qie, L.; Jiang, Y.; Huang, Y. H. Microwave-Induced in Situ Synthesis of Zn_2GeO_4/N-Doped Graphene Nanocomposites and Their Lithium-Storage Properties. *Chem.−Eur. J.* **2013**, *19*, 6027−6033.

(14) Park, M. H.; Kim, K.; Kim, J.; Cho, J. Flexible Dimensional Control of High-Capacity Li-Ion-Battery Anodes: From 0D Hollow to 3D Porous Germanium Nanoparticle Assemblies. *Adv. Mater.* **2010**, *22*, 415−418.

(15) Hu, C. G.; Xiao, Y.; Zhao, Y.; Chen, N.; Zhang, Z. P.; Cao, M. H.; Qu, L. T. Highly Nitrogen-Doped Carbon Capsules: Scalable Preparation and High-Performance Applications in Fuel Cells and Lithium Ion Batteries. *Nanoscale* **2013**, *5*, 2726−2733.

(16) Li, X. N.; Zhu, X. B.; Zhu, Y. C.; Yuan, Z. Q.; Si, L. L.; Qian, Y. T. Porous Nitrogen-Doped Carbon Vegetable-Sponges with Enhanced Lithium Storage Performance. *Carbon* **2014**, *69*, 515−524.

(17) Xiao, Y.; Wang, X.; Wang, W.; Zhao, D.; Cao, M. H. Engineering Hybrid between MnO and N-Doped Carbon to Achieve Exceptionally High Capacity for Lithium-Ion Battery Anode. *ACS Appl. Mater. Interfaces* **2014**, *6*, 2051−2058.

(18) Li, S. L.; Chen, C.; Fu, K.; White, R.; Zhao, C. X.; Bradford, P. D.; Zhang, X. W. Nanosized Ge@CNF, Ge@C@CNF and Ge@CNF@C Composites *via* Chemical Vapour Deposition Method for Use in Advanced Lithium-Ion Batteries. *J. Power Sources* **2014**, *253*, 366−372.

(19) Zhang, L.; Lou, X. W. Hierarchical MoS_2 Shells Supported on Carbon Spheres for Highly Reversible Lithium Storage. *Chem.−Eur. J.* **2014**, *20*, 5219−5223.

(20) Zhang, K. J.; Han, P. X.; Gu, L.; Zhang, L. X.; Liu, Z. H.; Kong, Q. S.; Zhang, C. J.; Dong, S. M.; Zhang, Z. Y.; Yao, J. H.; Xu, H. X.; Cui, G. L.; Chen, L. Q. Synthesis of Nitrogen-Doped MnO/Graphene Nanosheets Hybrid Material for Lithium Ion Batteries. *ACS Appl. Mater. Interfaces* **2012**, *4*, 658−664.

(21) Deifallah, M.; McMillan, P. F.; Cora, F. Electronic and Structural Properties of Two-Dimensional Carbon Nitride Graphenes. *J. Phys. Chem. C* **2008**, *112*, 5447−5451.

(22) Hwang, I. S.; Kim, J. C.; Seo, S. D.; Lee, S. J.; Lee, J. H.; Kim, D. W. A Binder-Free Ge-Nanoparticle Anode Assembled on Multiwalled Carbon Nanotube Networks for Li-Ion Batteries. *Chem. Commun.* **2012**, *48*, 7061−7063.

(23) Ren, J. G.; Wu, Q. H.; Tang, H.; Hong, G.; Zhang, W. J.; Le, S. T. Germanium−Graphene Composite Anode for High-Energy Lithium Batteries with Long Cycle Life. *J. Mater. Chem. A* **2013**, *1*, 1821−1826.

(24) Li, W. H.; Yang, Z. Z.; Cheng, J. X.; Zhong, X. W.; Gu, L.; Yu, Y. Germanium Nanoparticles Encapsulated in Flexible Carbon Nanofibers as Self-Supported Electrodes for High Performance Lithium-Ion Batteries. *Nanoscale* **2014**, *6*, 4532−4537.

(25) Chizari, K.; Vena, A.; Laurentius, L.; Sundararaj, U. The Effect of Temperature on the Morphology and Chemical Surface Properties of Nitrogen-Doped Carbon Nanotubes. *Carbon* **2014**, *68*, 369−379.

(26) Ghosh, K.; Kumar, M.; Maruyamaa, T.; Ando, Y. Controllable Growth of Highly N-Doped Carbon Nanotubes from Imidazole: A Structural, Spectroscopic and Field Emission Study. *J. Mater. Chem.* **2010**, *20*, 4128−4134.

(27) van Dommelea, S.; Romero-Izquirdoa, A.; Brydsonb, R.; de Jonga, K. P.; Bitter, J. H. Tuning Nitrogen Functionalities in Catalytically Grown Nitrogen-Containing Carbon Nanotubes. *Carbon* **2008**, *46*, 138−148.

(28) Li, N.; Liu, G.; Zhen, C.; Li, F.; Zhang, L.; Cheng, H. M. Battery Performance and Photocatalytic Activity of Mesoporous Anatase TiO_2 Nanospheres/Graphene Composites by Template-Free Self-Assembly. *Adv. Funct. Mater.* **2011**, *21*, 1717−1722.

(29) Li, H. B.; Kang, W. J.; Wang, L.; Yue, Q. L.; Xu, S. L.; Wang, H. S.; Liu, J. F. Synthesis of Three-Dimensional Flowerlike Nitrogen-Doped Carbons by a Copyrolysis Route and the Effect of Nitrogen Species on the Electrocatalytic Activity in Oxygen Reduction Reaction. *Carbon* **2013**, *54*, 249−257.

(30) Ferrari, A. C.; Robertson, J. Interpretation of Raman Spectra of Disordered and Amorphous Carbon. *Phys. Rev. B* **2000**, *61*, 14095−14107.

(31) Zhou, M.; Pu, F.; Wang, Z.; Guan, S. Y. Nitrogen-Doped Porous Carbons through KOH Activation with Superior Performance in Supercapacitors. *Carbon* **2014**, *68*, 185−194.

(32) Liu, M. X.; Gan, L. H.; Xiong, W.; Zhao, F. Q.; Fan, X. Z.; Zhu, D. Z.; Xu, Z. J.; Hao, Z. X.; Chen, L. W. Nickel-Doped Activated

Mesoporous Carbon Microspheres with Partially Graphitic Structure for Supercapacitors. *Energy Fuels* **2013**, *27*, 1168−1173.
(33) Mao, Y.; Duan, H.; Xu, B.; Zhang, L.; Hu, Y. S.; Zhao, C. C.; Wang, Z. X.; Chen, L. Q.; Yang, Y. S. Lithium Storage in Nitrogen-Rich Mesoporous Carbon Materials. *Energy Environ. Sci.* **2012**, *5*, 7950−7955.
(34) Mi, R.; Liu, H.; Wang, H.; Wong, K. W.; Mei, J.; Chen, Y. G.; Lau, W. M.; Yan, H. Effects of Nitrogen-Doped Carbon Nanotubes on the Discharge Performance of Li−Air Batteries. *Carbon* **2014**, *67*, 7447−7452.
(35) Dresselhaus, M. S.; Eelund, P. C. Phonons in Carbon Nanotubes. *Adv. Phys.* **2000**, *49*, 705−814.
(36) Xia, Y.; Xiao, Z.; Dou, X.; Huang, H.; Lu, X. H.; Yan, R. J.; Gan, Y. P.; Zhu, W. J.; Tu, J. P.; Zhang, W. K.; Tao, X. Y. Green and Facile Fabrication of Hollow Porous MnO/C Microspheres from Microalgaes for Lithium-Ion Batteries. *ACS Nano* **2013**, *7*, 7083−7092.
(37) Yang, X. Y.; Li, X. M.; Ma, X.; Jia, L.; Zhu, L. D. Carbonaceous Impurities GreatlyImpact on the Electrochemical Capacitance of Graphene. *RSC Adv.* **2013**, *3*, 6752−6755.
(38) Yang, J.; Bai, H. Z.; Tan, X. C.; Lian, J. S. IR and XPS Investigation of Visible-Light Photocatalysis—Nitrogen-Carbon-Doped TiO_2 Film. *Appl. Surf. Sci.* **2006**, *253*, 1988−1994.
(39) Zhao, L.; Hu, Y. S.; Li, H.; Wang, Z. X.; Chen, L. Q. Porous $Li_4Ti_5O_{12}$ Coated with N-Doped Carbon from Ionic Liquids for Li-Ion Batteries. *Adv. Mater.* **2011**, *23*, 1385−1388.
(40) Feng, S. S.; Li, W.; Shi, Q.; Li, Y. H.; Chen, J. C.; Ling, Y.; Asiri, A. M.; Zhao, D. Y. Synthesis of Nitrogen-Doped Hollow Carbon Nanospheres for CO_2 Capture. *Chem. Commun.* **2014**, *50*, 329−331.
(41) Tran, C.; Kalra, V. Fabrication of Porous Carbon Nanofibers with Adjustable Pore Sizes as Electrodes for Supercapacitors. *J. Power Sources* **2013**, *235*, 289−296.
(42) Tao, S. S.; Yue, W. B.; Zhong, M. Y.; Chen, Z. J.; Ren, Y. Fabrication of Graphene-Encapsulated Porous Carbon−Metal Oxide Composites as Anode Materials for Lithium-Ion Batteries. *ACS Appl. Mater. Interfaces* **2014**, *6*, 6332−6339.
(43) Xiao, Y.; Hu, C. W.; Cao, M. H. Facile Microstructure Control of Mesoporous $Co_{1.29}Ni_{1.71}O_4$ and the Effect of the Microstructure on Lithium-Storage Performance. *Chem.−Eur. J.* **2013**, *19*, 10193−10200.
(44) Li, D.; Seng, K. H.; Shi, D. Q.; Chen, Z. X.; Liu, H. K.; Guo, Z. P. A Unique Sandwich-Structured C/Ge/Graphene Nanocomposite as an Anode Material for High Power Lithium Ion Batteries. *J. Mater. Chem. A* **2013**, *1*, 14115−14121.
(45) Wang, Y.; Wang, G. X. Facile Synthesis of Ge@C Core−Shell Nanocomposites for High-Performance Lithium Storage in Lithium-Ion Batteries. *Chem. − Asian J.* **2013**, *8*, 3142−3146.
(46) Ren, J. G.; Wu, Q. H.; Tang, H.; Hong, G.; Zhang, W. J.; Lee, S. T. Germanium−Graphene Composite Anode for High-Energy Lithium Batteries with Long Cycle Life. *J. Mater. Chem. A* **2013**, *1*, 1821−1826.
(47) Wang, L. Y.; Zhou, L. H.; Zhang, C.; Zhao, F. Y. Supercritical Carbon Dioxide Assisted Deposition of Fe_3O_4 Nanoparticles on Hierarchical Porous Carbon and Their Lithium-Storage Performance. *Chem.−Eur. J.* **2014**, *20*, 4308−4315.
(48) Cao, C.; Zhang, J. *An Introduction to Electrochemical Impedance Spectroscopy*; Science Publications: Beijing, 2002; pp 86−106.
(49) Xiao, Y.; Hu, C. W.; Cao, M. H. High Lithium Storage Capacity and Rate Capability Achieved by Mesoporous Co_3O_4 Hierarchical Nanobundles. *J. Power Sources* **2014**, *247*, 49−56.
(50) Zhong, C.; Wang, J. Z.; Gao, X. W.; Wexler, D.; Liu, H. K. In Situ One-Step Synthesis of a 3D Nanostructured Germanium−Graphene Composite and its Application in Lithium-Ion Batteries. *J. Mater. Chem. A* **2013**, *1*, 10798−10804.
(51) Sun, Y. M.; Hu, X. L.; Luo, W.; Xia, F. F.; Huang, Y. H. Reconstruction of Conformal Nanoscale MnO on Graphene as a High-Capacity and Long-Life Anode Material for Lithium Ion Batteries. *Adv. Funct. Mater.* **2013**, *23*, 2436−2444.
(52) Ren, Y.; Armstrong, A. R.; Jiao, F.; Bruce, P. G. Influence of Size on the Rate of Mesoporous Electrodes for Lithium Batteries. *J. Am. Chem. Soc.* **2010**, *132*, 996−1004.
(53) Wang, Y.; Zhang, H. J.; Lu, L.; Stubbs, L. P.; Wong, C. C.; Lin, J. Designed Functional Systems from Peapod-Like Co@Carbon to Co_3O_4@Carbon Nanocomposites. *ACS Nano* **2010**, *4*, 4753−4761.
(54) Wang, J.; Wang, J. Z.; Sun, Z. Q.; Gao, X. W.; Zhong, C.; Chou, S. L.; Liu, H. K. A Germanium/Single-Walled Carbon Nanotube Composite Paper as a Free-Standing Anode for Lithium-Ion Batteries. *J. Mater. Chem. A* **2014**, *2*, 4613−4618.
(55) Zhang, C. J.; Pang, S. P.; Kong, Q. S.; Liu, Z. H.; Hu, H.; Jiang, W.; Han, P. X.; Wang, D.; Cui, G. L. An Elastic Germanium−Carbon Nanotubes−Copper Foam Monolith as an Anode for Rechargeable Lithium Batteries. *RSC Adv.* **2013**, *3*, 1336−1340.
(56) Wang, C. D.; Chui, Y. S.; Li, Y.; Chen, X. F.; Zhang, W. J. Binder-Free Ge-Three Dimensional Graphene Electrodes for High-Rate Capacity Li-Ion Batteries. *Appl. Phys. Lett.* **2013**, *103*, 253909−253913.
(57) Yoon, S.; Park, C. M.; Sohn, H. J. Electrochemical Characterizations of Germanium and Carbon-Coated Germanium Composite Anode for Lithium-Ion Batteries. *Electrochem. Solid-State Lett.* **2008**, *11*, A42−A45.
(58) Woo, S. H.; Choi, S. J.; Park, J. H.; Yoon, W. S.; Hwang, S. W.; Whang, D. Entangled Germanium Nanowires and Graphite Nanofibers for the Anode of Lithium-Ion Batteries. *J. Electrochem. Soc.* **2013**, *160*, A112−A116.
(59) Ren, Y.; Armstrong, A. R.; Jiao, F.; Bruce, P. G. Influence of Size on the Rate of Mesoporous Electrodes for Lithium Batteries. *J. Am. Chem. Soc.* **2010**, *132*, 996−1004.